

Structure and ligand binding site characteristics of the human P2Y₁₁ nucleotide receptor deduced from computational modelling and mutational analysis

Jacques Zylberg^{1,§}, Denise Ecke^{2,§}, Bilha Fischer^{1*} and Georg Reiser^{2*},

¹ Department of Chemistry, Gonda-Goldschmied Medical Research Center, Bar-Ilan University, Ramat-Gan 52900, Israel

² Institut für Neurobiochemie, Medizinische Fakultät, Otto-von-Guericke-Universität Magdeburg, Leipziger Strasse 44, 39120 Magdeburg, Germany

Short title:

Mutational analysis of human P2Y₁₁ nucleotide receptor

Key words: Nucleotide receptor, P2Y receptor, Molecular Dynamics, Virtual Screening, Mutagenesis

§ Both authors contributed equally to this work

* Authors for correspondence:

bfischer@mail.biu.ac.il. (B.F.) and georg.reiser@medizin.uni-magdeburg.de (G.R.)

Author for submission: Dr. G. Reiser

Abbreviations: EC₅₀ value, half-maximal response; EF, enrichment factor; EIA, Enzyme-linked-Immunoassay; EL, extracellular loop; GFP, green fluorescent protein; GPCR, G-protein coupled receptor; hP2Y-R, human P2Y receptor; MD, molecular dynamics;

Abstract

The P2Y₁₁-receptor (P2Y₁₁-R) is a less explored drug target. We computed a *h*P2Y₁₁-R homology model with two templates, bovine-rhodopsin (2.6Å resolution) and a *h*P2Y₁:ATP complex model. The *h*P2Y₁₁-R model was refined using molecular dynamics calculations and validated by virtual screening methods, with an enrichment factor of 5. Furthermore, mutational analyses of R106, E186, R268, R307 and A313 confirmed the adequacy of our *h*P2Y₁₁-R model and the computed ligand recognition mode. The E186A and R268A mutants reduced the potency of ATP by one and three orders of magnitude, respectively. The R106A and R307A mutants were functionally inactive. We propose that residues R106, R268, R307 and E186 are involved in ionic interactions with the phosphate moiety of ATP. R307 is possibly also H-bonded to N⁶ of ATP via the backbone carbonyl. Activity of ATP at the F109I mutant revealed that the proposed π -stacking of F109 with the adenine ring is a minor interaction. The mutation A313N, which is part of a hydrophobic pocket in the vicinity of the ATP-C2-position, partially explains the high activity of 2-MeS-ATP at P2Y₁-R as compared to the negligible activity at the P2Y₁₁-R. Inactivity of ATP at the Y261A mutant implies that Y261 acts as a molecular switch, as in other G-protein coupled receptors. Moreover, analysis of cAMP responses seen with the mutants showed that the efficacy of coupling of the P2Y₁₁-R to G_s is more variable than coupling to G_q. Our model also indicates that S206 forms an H-bond with Py and M310 interacts with the adenine moiety.

Introduction

P2 receptors are activated by extracellular nucleotides [1]. These receptors are divided into two groups: ligand-gated cation channels, classified as P2X receptors [2], and the P2Y receptors, coupled to G proteins [3]. P2Y-Rs can be further subdivided into two phylogenetic groups. One group comprises the *hP2Y*_{1,2,4,6,11}-Rs that are coupled mainly to phospholipase C. In the second group consisting of the *hP2Y*_{12,13,14}-Rs, the inhibition of adenylyl cyclase is triggered. *hP2Y*_{12,13} are classical nucleotide receptors, whereas *hP2Y*₁₄ is activated by UDP-glucose [4]. The *hP2Y*₁₁-R, however, is coupled to stimulation of both the adenylyl cyclase, and the phospholipase C pathways [5]. This is a unique feature amongst the P2Y-R family.

Out of the first P2Y-R subgroup, the *hP2Y*₁-R and *hP2Y*₁₁-R are exclusively activated by adenine nucleotides, ATP and ADP [5, 6], whereas the *P2Y*_{4,6}-Rs prefer uracil nucleotides [7]. Specifically, the *hP2Y*₆-R is selectively activated by UDP, and the *hP2Y*₄-R is activated mainly by UTP. The *hP2Y*₂-R seems not to discriminate between purine or pyrimidine nucleotides and is stimulated equipotently by ATP and UTP (see refs. in [8]).

Unlike the *hP2Y*₁-R, which is the most thoroughly investigated *hP2Y*-R, its closest homologue, the *hP2Y*₁₁-R, sharing 33% identity, has been far less studied [5]. To date, no mutational analyses of the *hP2Y*₁₁-Rs were reported. Likewise, the *hP2Y*₁₁-R has been scarcely studied by computational methods [9].

The *hP2Y*₁-R was modelled extensively by Moro et al. [10, 11]. These computational studies, supported by mutational analyses, suggested the residues involved in ligand binding. Arg128, Tyr136, Lys280 and Arg310 were reported to interact with the ATP phosphate moiety, while Ser314 and Arg310 were believed to interact with the adenine moiety. These authors also proposed His132, His277 and

Ser317 to be involved in H-bonds with the sugar moiety [10]. The homology model of the *hP2Y₁*-R described by Moro and co-workers was based on a bovine (b)-rhodopsin template and subsequently refined using a cross-docking approach [10].

Different computational and optimization techniques were applied later by Major et al. for the modelling of the *hP2Y₁*-R [12, 13]. Thus, we performed the optimization of the *hP2Y₁*-R model in an explicitly hydrated lipid bilayer (triphasic system) [12]. The binding-pocket in the *hP2Y₁*-R model was then optimized using a Monte-Carlo and molecular dynamics (MD) protocol. In this way, we could explain not only the molecular recognition determinants of ATP and synthetic analogues, but we also provided an explanation for the *hP2Y₁*-R diastereoselectivity [13].

The P2Y-R family is the subject of intense ongoing investigations because of its important influence in physiological processes and involvement in various diseases, varying from cystic fibrosis [14] to platelet secretion and aggregation disorders [15]. Specifically, the *hP2Y₁₁*-R was reported to play roles in the treatment of neutropenia [16], acute myocardial infarcts [17] and in the maturation process of dendritic cells [18].

In this study, we aimed to provide an accurate model of the *hP2Y₁₁*-R supported by mutational analyses to open the possibility of designing specific ligands for this receptor. By means of these investigations, we provide an insight into the ligand binding determinants of the *hP2Y₁₁*-R. The proposed ligand recognition mode is consistent with the pharmacological data.

Methods

Alignment

Multiple sequence alignment involving human(*h*)-P2Y₁₁-R has been performed using the ClustalW software [19]. The alignment included the following sequences originating from the NCBI database: *h*P2Y₁-R (gi:4505557), *h*P2Y₂-R (gi:28872720), *h*P2Y₄-R (gi:4505561), *h*P2Y₆-R (gi:14424758), *h*P2Y₁₁-R (gi:21263830) and b-rhodopsin (gi:129204) [20].

Modelling

Both b-rhodopsin crystallographic structure at 2.6Å resolution [21], and the *h*P2Y₁-R:ATP complex model [12], constructed previously, were used as templates to construct the *h*P2Y₁₁-R model. A set of 200 models with different energies were generated using the Modeler software [22], and the best one was selected. The models did not include any of the *h*P2Y₁₁-R's loops. Structural features known to be conserved, in G-protein coupled receptors (GPCRs) in general or in the *h*P2Y-R subfamily in particular, have been introduced using constraints during the construction of the *h*P2Y₁₁-R model. Thus, an ionic bridge, Asp196 and Arg275 in the *h*P2Y₁₁-R [11] was constrained. In addition, the TM backbones were constrained as α -helices to remove helical kinks specific to b-rhodopsin. In addition, α -helical constraints were introduced near the extra- and intracellular sides of the helices. These constraints prevent the helices from unwinding during optimization procedures in the building protocol of Modeler.

Model refinement

The best model obtained from the homology modelling was used here as a starting coordinated set. The receptor model consists of the helical bundle and the ATP molecule. Harmonic constraints (factor 15) have been imposed on the dihedral

angles of the peptide backbone. The dihedrals from the Pro residues in all TMs have not been included in these constraints. A distance constraint has been used in all molecular dynamics (MD) simulations, which prevented the ATP molecule from flipping or floating out of its binding-pocket. The helices' extremities have been capped using an acetyl group for C-terminals and methyl for the N-terminals. Blocking method has been adopted to remove interactions between the helices' termini and between some residues and the ATP molecule. The model has first been subjected to an extensive minimization using a combination of the steepest descent and conjugated derivatives algorithm (with energy tolerance 0.0001 Kcal/mol).

All MD calculations performed here use the Velocity Verlet integration algorithm as implemented in CHARMM (developmental version 31b1). The minimized model was heated from 0° K up to 300° K for 9 ps with a 5° K increment every 100 time steps (time step = 0.0015 ps). It has then been subjected to a 150 ps simulation. The latter was concluded with a minimization using the steepest descent algorithm with a 0.001 Kcal/mol energy tolerance.

The receptor relaxation could be easily monitored when tracking the overall system energy. No trajectory post-processing has been done. The relaxed receptor, except the binding-pocket, was then constrained. The radius pattern surrounding the ATP molecule followed a 6Å-10Å-∞ scheme (free-constrained-fixed). The ligand-receptor complex has been heated from 0°K to 900°K for 27 ps with a 5°K increment every 100 time steps (time step = 0.0015 ps) followed by 300 ps of simulation.

In order to retrieve relevant parameter values, the simulation has been quenched using a steepest descent minimization with 0.001 Kcal/mol energy tolerance for every recorded frame. Interaction energies between the ATP molecule and

selected residues have been extracted as well as the overall energy. The interval of the investigated frames counted 600 integration steps.

Average Structure

An average structure of the three most stable structures encountered during the simulation was calculated using the BLOCK facility in CHARMM [23] and further minimized with an energy tolerance of 0.0001 Kcal/mol.

Model Validation

The calculated *hP2Y₁₁*-R model was validated: A. by inspection of the geometrical parameters using the Ramachandran plot, B. by virtual screening.

A. The geometric parameters of the *hP2Y₁₁*-R model have been revised using the Ramachandran plot generated by ProCheck software [24]. More than 99 % of residues were classified in allowed regions, leaving one out of a total of 203 residues in a disallowed region.

B. The compound library created for the virtual screening included the following: seven known *hP2Y₁₁*-R agonists (Fig. 2) constructed and further optimized at AM1 level using the Gaussian98 [25]; a set of 42 nucleotides downloaded at random from the ChemBank online database [26] (Supplementary Material); the drug-like compounds library proposed by Accelrys [27], which contains 970 molecules.

The volume of the *hP2Y₁₁*-R binding pocket has been defined by the ATP molecule calculated based on the previously reported *hP2Y₁*-R:ATP complex model [12]. The model has been subjected to Surflex [28] routines in order to characterize the binding-pocket (creating the “protomol” using default parameters). The entire compound library has been docked in the *hP2Y₁₁*-R model, using the Surflex software [28]. The resulting output has been processed using advised parameter values (1.0 polarity penalty threshold; -3.0 penetration penalty threshold; 100 maximum allowed

rotatable bonds, as proposed by the Surflex documentation). The aptitude of the virtual screening was expressed in terms of enrichment factor (EF). The EF is the ratio of the database percentage containing the target molecules before (100%) and after ranking (DB%). $EF = 100\% / DB\%$.

Mutagenesis analysis

Site-directed mutagenesis was performed using the QuikChange Site-Directed Mutagenesis Kit (Stratagene, LaJolla, CA, USA). The DNA sequence of the *hP2Y₁₁*-R (GenBank™/EBI accession number AF030335) was kindly provided by Dr. D. Communi and placed between the EcoRI/BamHI restriction sites of the eGFPN1 vector (Clontech, Heidelberg). The mutations were introduced using customized oligonucleotides (Quiagen, Hilden) and confirmed by DNA sequencing. The P2Y₁₁-GFP (green fluorescent protein) receptor DNA and DNA carrying the respective mutation were used to transfect 1321N1 human astrocytoma cells. Cells were grown at 37°C in 10% CO₂ in high-glucose DMEM medium supplemented with 5% FCS, 100 U/ml penicillin, 100 IU/ml streptomycin (Seromed, Biochrom, Berlin) and transfected with the recombinant plasmids using FuGENE™ 6 transfection reagent (ratio Fugene:DNA 3:2) as given in the manufacturer's protocol (Roche, Mannheim, Germany). Transfected cells were selected with 0.5 mg/ml G418 (Calbiochem, La Jolla, CA, USA) for stable expression of the wild type and mutant receptors.

Stably transfected cells were plated on glass coverslips (Ø = 22 mm, OmniLab, Bremen, Germany), and single cell measurement was done after 3 days, when the cells were 30-50% confluent. The changes in free intracellular Ca²⁺ concentration ([Ca²⁺]_i) were measured, as described before [29] using the calcium indicator fura-2AM (Biomol, Hamburg/Molecular Probes) and recording the change in fluorescence intensity after stimulation with various agonists (Sigma, Deisenhofen,

Germany). The cells were imaged with a system from TILL Photonics (München) using a X40 oil immersion objective and a flow rate of 1 ml/min in a recording chamber containing 0.2 ml [30]. Calcium data were analyzed with the Excel program applying basal deduction to the calcium traces and calculating the peak height for each cell. Concentration-response data obtained with average values from 40 to 70 single cells were further analyzed to derive EC₅₀ values (half-maximal response) using the SigmaPlot program (Systat, Erkrath, Germany). Calculation of the EC₅₀ values and curve fitting were performed using the following equation with a standard slope: $y = R_{\min} + \frac{R_{\max} - R_{\min}}{1 + 10^{(\log EC_{50} - x)}}$, where the maximal response (R_{\max}) was adjusted to the top plateau of the ATP curve.

For cAMP measurements, stably transfected cells were seeded in 6-well plates at a density of 100.000 cells per well and grown for 2 days till 80% confluency was reached. Prior to stimulation, the medium was aspirated and replaced by Na-HBS buffer (HEPES buffered saline: 145 mM NaCl, 5.4 mM KCl, 1.8 mM CaCl₂, 1 mM MgCl₂, 25 mM glucose and 20 mM HEPES/ Tris pH 7.4) containing 0.5 M IBMX (isobutyl-methyl-xanthine) and 1 μM DPSPX (1,3-dipropyl-8-sulphophenyl-xanthine) an A₁/A₂ receptor antagonist. After 30 min incubation at 37°C in this buffer, cells were stimulated with ATP for 10 min. After stimulation, the buffer was aspirated and cells were washed with PBS and lysed with 0.1 M HCl containing 0.05 % Triton X-100. Lysates were harvested and a 100 μl aliquot kept for protein estimation. Tubes were centrifuged at 1000 x g for 10 min and supernatants were directly used for the assay. Determination of intracellular cAMP was done using the Direct cAMP EIA (Enzyme-linked-Immunoassay) kit (assay designs, Ann Arbor, Michigan, USA). Data were analyzed using Graph Pad Prism.

The expression levels of wild type and mutant receptors were analyzed by flow cytometry using a FACS LSR (BD Biosciences, Heidelberg). Cells were grown in 5 cm culture dishes (Nunc, Wiesbaden, Germany) to 80% confluency, harvested, and resuspended in culture medium. The expression levels of 10.000 cells were analyzed by determining the mean intensity (geometric median) of the GFP fluorescence per cell using the Flow Jo software.

Results and Discussion

Similarity and identity of *hP2Y₁₁*-R and *hP2Y₁*-R, and modelling of the *hP2Y₁₁*-R

The human (*h*)*P2Y₁₁*-R is characterized by considerably larger second and third extracellular loops (EL2 and EL3, respectively) as compared to other *hP2Y*-R subtypes and bovine (*b*)-rhodopsin (e.g., 35 amino acids (aa) vs. 25 aa for EL2, and 31 aa vs. 22 aa for EL3, as compared to the *hP2Y₁*-R). *b*-rhodopsin and the *hP2Y₁₁*-R share 21% sequence identity and 52% similarity in the transmembrane (TM) domains, whereas the *hP2Y₁*-R shares 38% identity and 72% similarity with the *hP2Y₁₁*-R in the TM domains (Table 1). The amino acid sequence of the *hP2Y₁₁*-R exhibits 33% overall amino acid identity with the *hP2Y₁* receptor, its closest homologue.

To model the *hP2Y₁₁*-R we first aligned the *hP2Y₁₁*-R TM regions with multiple sequences: *b*-Rhodopsin and the *hP2Y_{1,2,4,6}*-Rs. The alignment in the TM domains has no gaps except for a single residue gap that was introduced in the beginning of TM6 (Fig. 1). This negligible gap is far away from the putative binding site (see below) and is located at the flexible TM extremity. All the conserved residues of the GPCR family A, as mentioned by Mirzadegan *et al.* [31], were aligned correctly. This includes highly conserved residues as well as residues related to the known GPCR patterns such as (E/D)RY in TM3 and NPxxY in TM7 (Fig. 1) [31].

The model computed here for the *hP2Y₁₁*-R did not include any loops, as opposed to our previously reported *hP2Y₁*-R model [12]. This is due to the very flexible nature of the loops that prevents their accurate modelling. Furthermore, EL2 and EL3 in the *hP2Y₁₁*-R are significantly longer (9 and 19 amino acids, respectively) than those of *b*-rhodopsin and many related GPCRs [9]. Therefore, alignment and modeling of these loops is certainly unreliable. Computational study of only the

helical bundle of GPCRs has become a well established procedure [32]. b-rhodopsin at 2.6Å resolution [21] was used as a template to calculate the *hP2Y₁₁*-R model, despite the relatively low overall identity (<20%). Moreover, the *hP2Y₁*-R:ATP complex model [12] was used as an additional template, because of the high homology of the *hP2Y₁*-R with the *hP2Y₁₁*-R. The need for this model as a template arises as the experimental data (e.g. mutational analysis and pharmacological data) are scarce for the *hP2Y₁₁*-R, unlike for the *hP2Y₁*-R. Furthermore, the *hP2Y₁₁*-R-bound ATP was modelled based on *hP2Y₁*-R-bound ATP positioning [12].

For obtaining sufficiently accurate GPCR models, extensive optimization protocols are required. Therefore, our model was further subjected to a two-stage MD optimization protocol. At first, we optimized the helical bundle of the model by subjecting it to MD simulation without constraining the structure. The MD simulation lasted 150 ps. In the first 70 ps a full relaxation of the model by 300 Kcal/mol occurred. Previously reported MD simulation of the *hP2Y₁₁*-R [9] lasted only 50 ps, which we have found insufficient for a full relaxation of the receptor. The structural nuances which distinguish even closely related proteins are of utmost importance when e.g. subtype receptor selectivity has to be considered, which is the case here. The MD relaxation protocol lets those nuances come into play as we have demonstrated for the closely related *hP2Y₁*-R and *hP2Y₁₁*-R.

In the next step, the model was fixed while only the binding pocket area with a bound ATP molecule was subjected to a quenched dynamics simulation. The simulation revealed that the residues involved in ATP recognition have favourable interaction energies. Out of this simulation an average *hP2Y₁₁*-R:ATP structure was extracted.

To validate the calculated *hP2Y₁₁*-R models, they were subjected to a virtual screening study. This study used *hP2Y₁₁*-R agonists [5] (Fig. 2) as target molecules and a random nucleotides library (Supplementary Material) as well as a random drug-like set of molecules as decoy molecules [27]. When testing the agonist discrimination capabilities of the homology structure, the enrichment factor was 4. The average *hP2Y₁₁*-R structure model, calculated from the MD refinement protocols, had an improved agonist discrimination, which was quantified by an enrichment factor of approximately 5 (Fig. 3), thus validating the calculated *hP2Y₁₁*-R model.

Characteristics of the *hP2Y₁₁*-R helical bundle

A multitude of positively charged amino acid residues in the ELs and at the ends of the TM helices are apparently unique for the *hP2Y*-R family (Fig. 4). Together, the positively charged residues in the ELs may play a role in guiding the negatively charged nucleotide ligand into the binding site, as suggested by Moro *et al.* [11]. The *hP2Y₁₁*-R contains 27 Pro residues in total and 11 of them are located in the TM regions. TM3 is the only TM domain without a Pro residue. The *hP2Y₁₁*-R-unique Pro311 residue replaces a highly conserved Ser residue in the other *hP2Y*-Rs. Unlike this conserved Ser residue, Pro311 is not involved in ligand recognition.

The conserved proline residues of GPCRs in TMs 6 and 7 are present in both the *hP2Y₁*-R and the *hP2Y₁₁*-R (Fig. 1). The induced kink by the highly conserved proline in TM6 has a pivotal role in GPCR activation and is involved in TM6 conformational change [33].

One of the most conserved patterns in GPCRs is the TM7 (N/D)PxxY motif present at the intracellular end. The mutation of the Asp or the Asn residue was shown to affect the activation of the phospholipase C and the adenylyl cyclase pathway. For

instance, the mutation Asn322Ala in the β_2 adrenergic receptor resulted in complete uncoupling of the receptor [34]. Furthermore, Gales *et al.* demonstrated for the cholecystokinin-B GPCR that the Asn391 residue of the NPxxY motif plays an essential role in the activation of the G α protein [35].

The pattern occurring in *hP2Y*_{1,2,4,6}-Rs is DPxxY. Interestingly enough, in the *hP2Y*₁₁-R this pattern has not been conserved. Instead, one finds the segment HPxxY. This unique motif may imply an alternative G protein activation mechanism and thus requires further investigation.

The *hP2Y*₁₁-R binding pocket and ATP binding-mode

The *hP2Y*₁₁-R amino acid residues interacting with the ATP molecule include Arg106, Phe109, Ser206, Arg268, Arg307 and Met310 (Table 2, Fig. 5). The three positively charged residues probably interact electrostatically with the triphosphate moiety, while Ser206 may form an H-bond with P $_{\gamma}$. The adenine moiety possibly interacts with Phe109 via π -stacking interactions, as was observed for the *hP2Y*₁-R:ATP complex model. A suspected unique interaction of the *hP2Y*₁₁-R with the adenine moiety involves Met310. Divalent sulfur atoms, such as in methionine residues, have an electrophilic character and interact with electron rich rings [36-38]. Met310 is aligned to Ala313 in the *hP2Y*₁-R, which is not involved in ligand binding.

However, an important H-bonding interaction involving N1 and N⁶-adenine positions and Ser residues (e.g. Ser314 in the *hP2Y*₁-R) in *hP2Y*-Rs complexes, is missing in the *hP2Y*₁₁-R. In the latter receptor, instead of a Ser residue, Pro311 is present, which does not form any specific interactions with the adenine ring. No alternative residue was found to interact with the adenine N1 position in the *hP2Y*₁₁-R:ATP complex. In this way, an important binding interaction is lost in the *hP2Y*₁₁-R

as compared to the *hP2Y₁*-R. In addition, no specific interactions of *hP2Y₁₁*-R residues were observed with the ribose ring.

In general, the EL2 is believed to be part of the GPCR binding pocket [39], and thus involved in ligand recognition. The Asp204 (in EL2) in *hP2Y₁*-R has been found to be a critical residue [9]. Major *et al.* proposed that the ATP phosphate chain coordinates with a Mg²⁺ ion, which is in turn coordinated with Asp204 [13].

The EL2 in the *hP2Y₁₁*-R is considerably longer than that of the *hP2Y₁*-R (35 vs. 25 amino acid residues, respectively). Attempts to model this very long EL2 were unsuccessful. Hence, the role of a residue in *hP2Y₁₁*-R (tentatively Glu186), corresponding to Asp204 in the *hP2Y₁*-R, could not be investigated computationally.

Recognition of C2-substituted ATP analogues

C2-substituted ATP analogues, such as 2-MeS-ADP or 2-MeS-ATP, proved to be exceptionally potent at the *hP2Y₁*-R [40]. Yet, at the *hP2Y₁₁*-R these analogues proved to be extremely poor agonists [5]. However, AR-C67085 (2-PrS- β,γ -dichloromethylene-D-ATP, 1 Fig.2), was shown to be a potent agonist at the *hP2Y₁₁*-R [5]. These observations prompted us to explore a tentative binding pocket for the C2-substituents of ATP. In both the *hP2Y₁*-R and the *hP2Y₁₁*-R models, a hydrophobic pocket is located in the vicinity of the ATP C2 position (Fig. 6). That pocket in the *hP2Y₁₁*-R is situated between TM2 and TM7, and is confined by residues Leu82 (TM2), Phe109 (TM3), Leu113 (TM3), Pro311 (TM7) and Ala313 (TM7). In our virtual screening study, C2-thioether substitutions such as MeS, EtS, PrS, BuS fitted into the *hP2Y₁₁*-R hydrophobic pocket. However, bulkier substitutions such as 2-tBuS and 2-neopentylS did not fit. Indeed, the 2-neopentylS-ATP analogue which was subsequently tested at the *hP2Y₁₁*-GFP receptor to stimulate intracellular

calcium release, showed no significant increase in the calcium level at concentrations up to 10 μ M.

However, the reduced potency of 2-MeS-ATP at the *h*P2Y₁₁-R as compared to ATP remains unresolved by virtual screening study and might be due to other reasons than poor fitting.

Site-directed mutagenesis of the *h*P2Y₁₁-R

Based on the *h*P2Y₁₁-R model proposed here, we next tested the binding mode hypothesis by mutating amino acid residues Arg106 (TM3), Phe109 (TM3), Glu186 (EL2), Arg268 (TM6) and Arg307 (TM7). 1321N1 cells were used to stably express the wild type and the mutant receptors, respectively. All receptors were constructed as GFP fusion proteins. The expression level was analyzed by flow cytometry detecting the GFP fluorescence intensity per cell. Both, wild type and mutant receptors displayed comparable fluorescence intensities. Some mutants (E186A, R268A) showed even a higher expression and other mutants (R106A, Y261A, and R307A) had around 80% expression level as compared to the wild type receptor (Table 3). The subcellular localization of the mutant receptors was examined by confocal microscopy. It was found to be comparable to that of the unmutated receptor for the E186A, R268A, R268Q, A313N mutant receptors. Although the F109I mutant receptor was only partially located at the plasma membrane, it exhibited a significant potency for ATP. Similar observations were made in a different mutagenesis approach, where even a 90% reduction in surface expression levels of the wild type *h*P2Y₁-R had no significant influence on the EC₅₀ values of the investigated agonist [41]. Therefore, the potency of ATP found at the F109I mutant as well as the potency

at the mutants with a similar subcellular localization (R106A, Y261A, and R307A) likely reflects the intrinsic activity of these constructs.

Functional activity of the receptors was determined, firstly, by monitoring the intracellular $[Ca^{2+}]_i$ release in the stably transfected cells and, secondly, by measuring cAMP accumulation induced after agonist stimulation. We employed the calcium indicator fura-2 and a cAMP-EIA, as described in Methods.

The two arginine residues in TM3 (Arg106) and TM7 (Arg307) were found to be most critical for *hP2Y₁₁*-R activation. After mutation to alanine, the ability of ATP to trigger a calcium signal at these receptors was almost abolished. Only at concentrations ≥ 10 mM an increase in calcium levels could be observed (Table 3). This confirms the hypothesis that these arginine residues stabilize the bound ATP through electrostatic interaction with ATP- P_α and P_γ of the phosphate moiety (Fig. 5). Besides the interaction with ATP- P_α , Arg307 is also believed to take part in an H-bond through its backbone carbonyl with N⁶. The corresponding residues in the *hP2Y₁* receptor (Arg128, Arg310) are similarly essential for ligand recognition. Their mutation resulted in functionally inactive receptors [42]. A model of the *hP2Y₆* receptor showed the involvement of these conserved arginine residues in binding of the phosphate moiety of the nucleotide to the receptor [43]. Surprisingly, at the *hP2Y₂* receptor only the mutation of the corresponding arginine in TM7 (Arg292) resulted in loss of function of the receptor, but mutation of the arginine in TM3 (Arg110) to leucine had little effect on the potency of the agonists [44]. The arginine in TM7 is part of a conserved motif (Q/KxxR) within the G_q -coupled subgroup of P2Y receptors. This motif is considered important for receptor activation.

The aromatic amino acid in TM3 (Phe109) that was thought to possibly interact with the adenine moiety via π -stacking interaction seems to be not very

critical for receptor activation. The EC₅₀ value was increased only by a factor of 4 after mutation of phenylalanine to isoleucine. Thus, there was no major effect on the potency of ATP at the receptor (Table 3, Fig. 7). However, this phenylalanine is highly conserved throughout the P2Y receptor family (Fig. 1). In the *h*P2Y₁ receptor, mutation of this residue to alanine caused a loss in potency for 2-MeS-ADP of about one order of magnitude, but it was still less critical for ligand recognition than other sites of the receptor [10, 42]. Moreover, this phenylalanine is possibly involved in hydrophobic interactions with the uracil ring of docked UDP in a molecular model of the *h*P2Y₆ receptor [43]. The mutation of Phe109 to isoleucine in the *h*P2Y₁₁ receptor did probably not much disturb the recognition of ATP at the receptor, since isoleucine is also a bulky, hydrophobic amino acid and therefore loss in potency was only 4-fold. Thus, the prediction of π -stacking between the adenine and the phenyl ring could not be verified experimentally.

The role of the ELs for nucleotide binding by P2Y-Rs has been suggested previously [41]. Furthermore, the importance of the EL2 Asp204 residue in ligand recognition has been already shown for the *h*P2Y₁-R [9, 13]. Glu186 was a residue in the EL2 of the *h*P2Y₁₁-R predicted to be involved in ligand recognition. Mutation of this glutamate to alanine resulted in a decreased potency of ATP at the receptor. The shift was more than one order of magnitude (Table 3, Fig. 7), consistent with the finding at the *h*P2Y₁-R. However, for the more potent *h*P2Y₁₁-R agonist ATP γ S the shift in potency was only 5-fold, compared to the wild type receptor. This implies that Glu186 interacts with phosphates P $_{\alpha}$ and P $_{\beta}$ of the triphosphate moiety, probably also via coordination of a Mg²⁺ ion as proposed for the corresponding residue in the *h*P2Y₁-R [13]. The relatively small shift in potency for agonists at the Glu186 mutant

implies a modulatory function of this residue in receptor functionality, as proposed for the corresponding residue in the *hP2Y₁*-R [11, 41].

The Arg268 residue that was thought to be involved in ATP-P_β recognition is part of a conserved motif in TM6. For members belonging to the G_q-coupled subgroup of P2Y receptors the motif is HxxR/K, the G_i-coupled receptors have all arginine and not lysine. P1 receptors lack these arginine/ lysine residues, indicating the role of the positively charged amino acids in coordination of the phosphate moiety.

The Arg268Ala mutant receptor displayed a clearly reduced potency for ATP, compared to the wild type receptor (Table 3, Fig. 7), indicating the significance of an intact motif in TM6. When this arginine was substituted by glutamine, the potency of ATP at this receptor could be partially rescued (Table 3, Fig. 7). These findings are consistent with the interpretation of a partial recovery of the Arg268 interaction with ATP-P_β, which results in the partially restored activity. However, we cannot ignore the importance of a conserved pattern in TM6. Indeed, it has been suggested that at least one mechanism of GPCR activation originates in TM6, being the "aromatic zipper" [45]. Although in cases where that mechanism of activation is clearly missing, we cannot rule out the existence of alternative mechanisms, which could involve Arg268. For both mutant receptors the change in potency for ATP_γS compared to the wild type receptor was not as drastic as for ATP, indicating that the major interaction is with P_β and a favourable interaction with P_γ-S, as compared to P_γ-O, still remains in the mutant. This favourable interaction may be due to a tighter fit of the larger P_γ-S moiety, compared to the phosphate moiety. The corresponding residues in the *hP2Y₁*-R (Lys280) and the *hP2Y₂*-R (Arg265) were also found to be essential for activation at low ATP concentrations, because a clear decrease in potency was found by

substitution of Lys280 or Arg265 by uncharged amino acids [42, 44]. In the *hP2Y₆*-R model, this position (Lys259) was part of a positively charged subpocket that bound the phosphate moiety of docked UDP [43], again highlighting the importance of this residue. For a member of the G_i-coupled subgroup of P2Y receptors the *hP2Y₁₂*-R, the significance of this arginine residue in TM6 was also confirmed [15, 46, 47].

The importance of a tyrosine residue in TM6 for ligand recognition was also investigated by means of mutagenesis. Tyr261 was not found to be directly interacting with the ATP molecule docked in our *hP2Y₁₁*-R model. However, it has been shown that a comparable residue (Tyr273) in the *hP2Y₁*-R located at the same position (6.48) seems to act as a molecular switch for receptor activation [9]. A Tyr273Ala mutation led to a functionally inactive receptor that was still able to bind agonist/antagonist with the same affinity as the wild type receptor. This is in accordance with the "aromatic zipper" theorem proposing a probable mechanism of activation. As it was suggested that this residue might also be important for other GPCRs, we generated a Tyr261Ala mutant *hP2Y₁₁*-R. The mutant receptor was incapable of being activated by ATP at concentrations ≤ 10 mM. Therefore, this tyrosine seems to play an important role in *hP2Y₁₁*-R activation. We assume that Tyr261 is solely involved in receptor activation, since it was not found to be binding the ATP significantly in any of our models. Due to the lack of a selective radioligand at the *hP2Y₁₁*-R we were not able to directly prove this suggestion.

At the entrance to the hydrophobic pocket located in the vicinity of the C2 position of ATP in the *hP2Y₁₁*-R model (Fig. 6A) an alanine residue (Ala313) is situated. This Ala313 is a unique feature of the *hP2Y₁₁*-R, as all other *hP2Y* receptors have an asparagine amino acid at this position. We expected that this Ala313 might have an impact on the reduction in potency for C2-substituted ATP derivatives at the

hP2Y₁₁-R [5, 48]. At the Ala313Asn mutant receptor, ATP was 2-fold less potent (Table 3, Fig. 7). However, 2-MeS-ATP ($EC_{50} = 8.37 \pm 2.05 \mu\text{M}$, $n=8$) displayed a gain in potency as compared to the wild type receptor ($EC_{50} = 11.1 \pm 6.30 \mu\text{M}$, $n=3$). This finding supports our hypothesis of this residue being a key player in the interactions involving ATP-C2 substitutions.

The *hP2Y₁₁*-R is also coupled to the activation of the adenylyl cyclase, besides induction of intracellular calcium release. Thus, we also investigated the ability of the receptor mutants to induce cAMP production upon stimulation. The mutants that showed no calcium responses were not considered.

The *hP2Y₁₁*-R expressed in 1321N1 cells was found to have a low efficacy in coupling to G_s [5]. Stimulation with ATP promoted cAMP accumulation with a 15-fold lower potency than IP_3 accumulation in these cells [49]. Therefore, we investigated the induction of agonist-induced [cAMP] increase for two relevant ATP concentrations (Fig. 8). The unmutated *hP2Y₁₁*-R caused a significant [cAMP] increase already at 100 μM ATP that was 80% of the maximum response seen at 1 mM ATP. There, the response reaches already the plateau-phase [49]. For the F109I and A313N receptor mutants we obtained similar results, supporting the notion of a minor influence of these residues on the potency of ATP, as also observed in the calcium measurements. However, the maximal increase in intracellular [cAMP] was much lower than in cells expressing the wild type receptor, suggesting that the phenylalanine residue in TM3 and the alanine residue in TM7 are important for efficient coupling of the receptor to G_s . A strong influence on the cAMP response maxima was also found for a point-mutation in the glucagon receptor. Mutation of a phenylalanine to alanine in TM2 of the glucagon receptor lead to a reduced maximal response without affecting the EC_{50} value of the agonist [50].

In contrast, the glutamate in EL2 of the *hP2Y₁₁*-R seems to play a role in regulating the agonist potency and activity of the receptor. After mutation to alanine the agonist-induced [cAMP] increase was much stronger as compared to the rise with the wild type receptor. Stimulation with 1 mM ATP resulted in a 3-fold higher cAMP content than in cells expressing the unmutated *hP2Y₁₁*-R. The influence of the E186A mutation on the potency of ATP could not be easily quantified in the [cAMP] measurements. It was not clear, whether at 1 mM ATP the maximum response was reached. Attempts of using higher concentrations were unsuccessful because at 10 mM ATP an interference with the cAMP response of the *hP2Y₁₁*-R by other mechanisms took place (data not shown). However, the E186A mutant seems to display a reduced potency in activating adenylyl cyclase.

Similar observations were made when the cAMP accumulation after ATP stimulation was investigated in 1321N1 cells expressing the R268A receptor mutant. At 100 μ M ATP no increase in the cAMP content was found compared to basal levels whereas at 1 mM cells responded like control cells. This reflects the drastically reduced potency of ATP at this receptor mutant as found in the calcium measurements described above. The cells expressing the R268Q receptor mutant showed even higher [cAMP] values after stimulation with 1 mM ATP than the wild type *hP2Y₁₁*-R-1321N1 cells. For both, the R268A and R268Q receptor mutants, maximal stimulation could not be established, as already described.

Thus, the E186A and R268A,Q receptor mutants seem to be more efficiently coupled to the activation of adenylyl cyclase compared to the wild type *hP2Y₁₁*-R. A similar phenomenon was observed in other GPCR mutants. Mutation of polar residues to alanine in TM6 and TM7 of the glucagon receptor resulted in increased response maxima to glucagon-NH₂ [50]. The β_1 receptor carrying a point-mutation in TM2 and

the TSH receptor with a naturally occurring mutation in TM1 displayed both a more pronounced basal activity and higher cAMP accumulation after agonist stimulation, compared to the respective wild type receptors [51, 52].

Taken together, the analysis of G_s coupling reveals similar changes in agonist potency in the mutated $hP2Y_{11}$ -Rs as compared to G_q coupling. Moreover, specific residues in the $hP2Y_{11}$ -R seem to be important for controlling the stimulatory extent of cAMP-dependent processes.

Conclusions

The $hP2Y_{11}$ -R model calculated here has proven to be adequate for the investigation of the molecular recognition of this receptor. The computed models, which were extensively refined by MD simulation protocols, were not only able to reproduce experimental data but also to predict the affinity of previously untested ligands. We have found that the binding pockets of the $hP2Y_1$ -R and the $hP2Y_{11}$ -R are very similar. We have established that in the $hP2Y_{11}$ -R the residues involved in ligand binding are Arg106, Phe109, Ser206, Arg268, Arg307 and Met310. The involvement of Arg106, Tyr261, Arg268, Arg307 and Ala313 in ligand recognition was confirmed by a mutational study. Glu186 in the EL2 of the $hP2Y_{11}$ -R, aligned with the critical Asp204 in the $hP2Y_1$ -R, also proved significant for ligand recognition. Furthermore, mutation of Phe109, Glu186, Arg268, and Ala313 influences coupling of the $hP2Y_{11}$ -R to G_s , whereas the extent of coupling to G_q remains unaffected.

Only minor amino acid residue variations were observed in the binding site of $hP2Y_{11}$ -R as compared to $hP2Y_1$ -R (e.g. Pro311 vs. Ser314, in $P2Y_{11}$ - vs. $P2Y_1$ -R). In the $hP2Y_{11}$ -R, His317 appears instead of Asp in the conserved DPxxY motif in TM7,

a typical motif for all other P2Y-Rs. This new motif which may trigger a different mechanism of activation, is worth further investigations.

Although the *h*P2Y₁₁-R has a hydrophobic binding-pocket at the vicinity of the C2-position of ATP, similar to that of *h*P2Y₁-R (Fig. 6), the significantly lower activity of 2-MeS-ATP at *h*P2Y₁₁-R may be due to the lack of H-binding interactions which are present in the *h*P2Y₁-R. Specifically, the Ser314 in the *h*P2Y₁-R is probably involved in H-bonding interactions with the sulfur atom of 2-MeS-ATP [12, 13]. Therefore, we propose that the natural mutation of Ser314 as well as Asn316 in the *h*P2Y₁-R to Pro311 and A313 in the *h*P2Y₁₁-R, as compared to other *h*P2Y-Rs, could be responsible for the lower potency of 2-MeS-ATP as compared to ATP at the *h*P2Y₁₁-R.

Acknowledgements

We thank Dr. T. Hanck and Dr. F. Sedehizadeh for helpful suggestions in the mutagenesis experiments and Ms. D. Terhardt for technical help in the complete experimental study. We thank Dr. R. Hartig (Institute of Immunology, Medical Faculty Magdeburg) for providing the facilities to carry out flow cytometry analysis. BF and JZ thank Mr. M. Amitai (Department of Pharmaceutical Chemistry, School of Pharmacy, Hebrew University, Jerusalem) for helpful discussions.

References

- 1 Burnstock, G. (1972) Purinergic nerves. *Pharmacol. Rev.* **24**, 509-581
- 2 Abbracchio, M. P. and Burnstock, G. (1994) Purinoceptors: are there families of P2X and P2Y purinoceptors? *Pharmacol Ther.* **64**, 445-475
- 3 Fredholm, B. B., Abbracchio, M. P., Burnstock, G., Daly, J. W., Harden, T. K., Jacobson, K. A., Leff, P. and Williams, M. (1994) Nomenclature and classification of purinoceptors. *Pharmacol. Rev.* **46**, 143-156.
- 4 Chambers, J. K., Macdonald, L. E., Sarau, H. M., Ames, R. S., Freeman, K., Foley, J. J., Zhu, Y., McLaughlin, M. M., Murdock, P., McMillan, L., Trill, J., Swift, A., Aiyar, N., Taylor, P., Vawter, L., Naheed, S., Szekeres, P., Hervieu, G., Scott, C., Watson, J. M., Murphy, A. J., Duzic, E., Klein, C., Bergsma, D. J., Wilson, S. and Livi, G. P. (2000) A G protein-coupled receptor for UDP-glucose. *J. Biol. Chem.* **275**, 10767-10771
- 5 Communi, D., Robaye, B. and Boeynaems, J.-M. (1999) Pharmacological characterization of the human P2Y₁₁ receptor. *Br. J. Pharmacol.* **128**, 1199-1206
- 6 Webb, T. E., Simon, J., Krishek, B. J., Bateson, A. N., Smart, T. G., King, B. F., Burnstock, G. and Barnard, E. A. (1993) Cloning and functional expression of a brain G-protein-coupled ATP receptor. *FEBS Lett.* **324**, 219-225
- 7 Jacobson, K. A., Jarvis, M. F. and Williams, M. (2002) Purine and Pyrimidine (P2) Receptors as Drug Targets. *J. Med. Chem.* **45**, 4057-4093
- 8 von Kugelgen, I. (2006) Pharmacological profiles of cloned mammalian P2Y-receptor subtypes. *Pharmacol Ther.* **110**, 415-432
- 9 Costanzi, S., Mamedova, L., Gao, Z.-G. and Jacobson, K. A. (2004) Architecture of P2Y nucleotide receptors: Structural comparison based on sequence analysis, mutagenesis, and homology modeling. *J. Med. Chem.* **47**, 5393-5404
- 10 Moro, S., Guo, D., Camaioni, E., Boyer, J. L., Harden, T. K. and Jacobson, K. A. (1998) Human P2Y₁ receptor: molecular modeling and site-directed mutagenesis as tools to identify agonist and antagonist recognition sites. *J. Med. Chem.* **41**, 1456-1466

- 11 Moro, S., Hoffmann, C. and Jacobson, K. A. (1999) Role of the Extracellular Loops of G Protein-Coupled Receptors in Ligand Recognition: A Molecular Modeling Study of the Human P2Y₁ Receptor. *Biochemistry* **38**, 3498-3507
- 12 Major, D. T. and Fischer, B. (2004) Molecular recognition in purinergic receptors. 1. A comprehensive computational study of the h-P2Y₁-receptor. *J. Med. Chem.* **47**, 4391-4404
- 13 Major, D. T., Nahum, V., Wang, Y., Reiser, G. and Fischer, B. (2004) Molecular recognition in purinergic receptors. 2. Diastereoselectivity of the h-P2Y₁-receptor. *J. Med. Chem.* **47**, 4405-4416
- 14 Buescher, R., Hoerning, A., Patel, H. H., Zhang, S., Arthur, D. B., Grasemann, H., Ratjen, F. and Insel, P. A. (2006) P2Y₂ receptor polymorphisms and haplotypes in cystic fibrosis and their impact on Ca²⁺ influx. *Pharmacogenetics and Genomics* **16**, 199-205
- 15 Cattaneo, M. (2006) The P2 receptors and congenital platelet function defects. *Semin. Thromb. Hemost.* **32**, 77
- 16 Boeynaems, J.-M., Robaye, B., Janssens, R., Suarez-Huerta, N. and Communi, D. (2001) Overview of P2Y receptors as therapeutic targets. *Drug Dev. Res.* **52**, 187-189
- 17 Amisten, S., Melander, O., Wihlborg, A., Berglund, G. and Erlinge, D. (2006) Increased risk of acute myocardial infarction and elevated levels of C-reactive protein in carriers of the Thr87 variant of the ATP receptor P2Y₁₁. *Purinergic Signalling* **2**, 234-235
- 18 Wilkin, F., Duhant, X., Bruyns, C., Suarez-Huerta, N., Boeynaems, J. M. and Robaye, B. (2001) The P2Y₁₁ receptor mediates the ATP-induced maturation of human monocyte-derived dendritic cells. *J Immunol* **166**, 7172-7177
- 19 Thompson, J. D., Gibson, T. J., Plewniak, F., Jeanmougin, F. and Higgins, D. G. (1997) The CLUSTAL_X windows interface: flexible strategies for multiple sequence alignment aided by quality analysis tools. *Nucleic Acids Res.* **25**, 4876-4882.
- 20 NCBI. <http://www.ncbi.nlm.nih.gov/>
- 21 Okada, T., Fujiyoshi, Y., Silow, M., Navarro, J., Landau, E. M. and Shichida, Y. (2002) Functional role of internal water molecules in rhodopsin revealed by x-ray crystallography. *Proc. Natl. Acad. Sci. U S A* **99**, 5982-5987

- 22 Sali, A. and Blundell, T. L. (1993) Comparative protein modelling by satisfaction of spatial restraints. *J. Mol. Biol.* **234**, 779-815.
- 23 Brooks, B. R., Bruccoleri, R. E., Olafson, B. D., States, D. J., Swaminathan, S. and Karplus, M. (1983) CHARMM: a program for macromolecular energy, minimization, and dynamics calculations. *J. Comput. Chem.* **4**, 187-217
- 24 Laskowski, R. A., MacArthur, M. W., Moss, D. S. and Thornton, J. M. (1993) PROCHECK: a program to check the stereochemical quality of protein structures. *J. Appl. Crystallogr.* **26**, 283-291
- 25 Frisch, M. J., Trucks, G. W., Schlegel, H. B., Scuseria, G. E., Robb, M. A., Cheeseman, J. R., Zakrzewski, V. G., Montgomery, J. A., Jr, Stratmann, R. E., Burant, J. C., Dapprich, S., Millam, J. M., Daniels, A. D., Kudin, K. N., Strain, M. C., Farkas, O., Tomasi, J., Barone, V., Cossi, M., Cammi, R., Mennucci, B., Pomelli, C., Adamo, C., Clifford, S., Ochterski, J., Petersson, G. A., Ayala, P. Y., Cui, Q., Morokuma, K., Malick, D. K., Rabuck, A. D., Raghavachari, K., Foresman, J. B., Cioslowski, J., V. O. J., Baboul, A. G., Stefanov, B. B., Liu, G., Liashenko, A., Piskorz, P., Komaromi, I., Gomperts, R., Martin, R. L., Fox, D. J., Keith, T., Al-Laham, M. A., Peng, C. Y., Nanayakkara, A., Gonzalez, C., Challacombe, M., Gill, P. M. W., Johnson, B., Chen, W., Wong, M. W., Andres, J. L., Gonzalez, C., Head-Gordon, M., Replogle, E. S. and Pople, J. A. (1998), Gaussian, Inc., Pittsburgh
- 26 ChemBank. <http://chembank.med.harvard.edu>
- 27 Accelrys. <http://www.accelrys.com/reference/cases/studies/randomset.html>
- 28 Jain, A. N. (2003) Surflex: fully automatic flexible molecular docking using a molecular similarity-based search engine. *J. Med. Chem.* **46**, 499-511
- 29 Ubl, J. J., Vöhringer, C. and Reiser, G. (1998) Co-existence of two types of $[Ca^{2+}]_i$ -inducing protease-activated receptors (PAR-1 and PAR-2) in rat astrocytes and C6 glioma cells. *Neuroscience* **86**, 597-609
- 30 Vöhringer, C., Schäfer, R. and Reiser, G. (2000) A chimeric rat brain P2Y₁ receptor tagged with green-fluorescent protein: high-affinity ligand recognition of adenosine diphosphates and triphosphates and selectivity identical to that of the wild-type receptor. *Biochem. Pharmacol.* **59**, 791-800
- 31 Mirzadegan, T., Benko, G., Filipek, S. and Palczewski, K. (2003) Sequence Analyses of G-Protein-Coupled Receptors: Similarities to Rhodopsin. *Biochemistry* **42**, 2759-2767

- 32 Shacham, S., Topf, M., Avisar, N., Glaser, F., Marantz, Y., Bar-Haim, S., Noiman, S., Naor, Z. and Becker, O. M. (2001) Modeling the 3D structure of GPCRs from sequence. *Med. Res. Rev.* **21**, 472-483
- 33 Visiers, I., Ebersole, B. J., Dracheva, S., Ballesteros, J., Sealton, S. C. and Weinstein, H. (2002) Structural motifs as functional microdomains in G-protein-coupled receptors: energetic considerations in the mechanism of activation of the serotonin 5-HT_{2A} receptor by disruption of the ionic lock of the arginine cage. *Int. J. Quantum Chem.* **88**, 65-75
- 34 Barak, L. S., Menard, L., Ferguson, S. S., Colapietro, A. M. and Caron, M. G. (1995) The conserved seven-transmembrane sequence NP(X)₂Y of the G-protein-coupled receptor superfamily regulates multiple properties of the beta 2-adrenergic receptor. *Biochemistry* **34**, 15407-15414
- 35 Gales, C., Kowalski-Chauvel, A., Dufour, M. N., Seva, C., Moroder, L., Pradayrol, L., Vaysse, N., Fourmy, D. and Silvente-Poirot, S. (2000) Mutation of Asn-391 within the conserved NPXXY motif of the cholecystokinin B receptor abolishes Gq protein activation without affecting its association with the receptor. *J. Biol. Chem.* **275**, 17321-17327.
- 36 Zauhar, R. J., Colbert, C. L., Morgan, R. S. and Welsh, W. J. (2000) Evidence for a strong sulfur-aromatic interaction derived from crystallographic data. *Biopolymers* **53**, 233-248
- 37 Pal, D. and Chakrabarti, P. (2001) Non-hydrogen bond interactions involving the methionine sulfur atom. *J. Biomol. Struct. Dyn.* **19**, 115-128.
- 38 Tatko, C. D. and Waters, M. L. (2004) Investigation of the nature of the methionine-p interaction in b-hairpin peptide model systems. *Protein Science* **13**, 2515-2522
- 39 Palczewski, K., Kumasaka, T., Hori, T., Behnke, C. A., Motoshima, H., Fox, B. A., Le Trong, I., Teller, D. C., Okada, T., Stenkamp, R. E., Yamamoto, M. and Miyano, M. (2000) Crystal structure of rhodopsin: A G protein-coupled receptor. *Science* **289**, 739-745
- 40 Palmer, R. K., Boyer, J. L., Schachter, J. B., Nicholas, R. A. and Harden, T. K. (1998) Agonist action of adenosine triphosphates at the human P2Y₁ receptor. *Mol. Pharmacol.* **54**, 1118-1123
- 41 Hoffmann, C., Moro, S., Nicholas, R. A., Harden, T. K. and Jacobson, K. A. (1999) The role of amino acids in extracellular loops of the human P2Y₁

- p>receptor in surface expression and activation processes.
- J. Biol. Chem.*
- 274**
- , 14639-14647
- 42 Jiang, Q., Guo, D., Lee, B. X., Van Rhee, A. M., Kim, Y. C., Nicholas, R. A., Schachter, J. B., Harden, T. K. and Jacobson, K. A. (1997) A mutational analysis of residues essential for ligand recognition at the human P2Y₁ receptor. *Mol. Pharmacol.* **52**, 499-507
 - 43 Costanzi, S., Joshi, B. V., Maddileti, S., Mamedova, L., Gonzalez-Moa, M. J., Marquez, V. E., Harden, T. K. and Jacobson, K. A. (2005) Human P2Y₆ receptor: molecular modeling leads to the rational design of a novel agonist based on a unique conformational preference. *J. Med. Chem.* **48**, 8108-8111
 - 44 Erb, L., Garrad, R., Wang, Y., Quinn, T., Turner, J. T. and Weisman, G. A. (1995) Site-directed mutagenesis of P2U purinoceptors. Positively charged amino acids in transmembrane helices 6 and 7 affect agonist potency and specificity. *J. Biol. Chem.* **270**, 4185-4188
 - 45 Rosenkilde, M. M., Andersen, M. B., Nygaard, R., Frimurer, T. M. and Schwartz, T. W. (2006) Activation of the CXCR3 chemokine receptor through anchoring of a small molecule chelator ligand between TM-III, -IV and -VI. *Mol. Pharmacol.*, 2006 Dec 2014; [Epub ahead of print]
 - 46 Cattaneo, M., Zighetti, M. L., Lombardi, R., Martinez, C., Lecchi, A., Conley, P. B., Ware, J. and Ruggeri, Z. M. (2003) Molecular bases of defective signal transduction in the platelet P2Y₁₂ receptor of a patient with congenital bleeding. *Proc. Natl. Acad. Sci. U S A* **100**, 1978-1983
 - 47 Hoffmann, K. A. and von Kügelgen, I. (2006) Evidence for the involvement of basic amino acid residues in transmembrane regions 6 and 7 of the human platelet P2Y₁₂-receptor in ligand recognition. *Purinergic Signalling* **2**, 199-200
 - 48 Ecke, D., Tulapurkar, M. E., Nahum, V., Fischer, B. and Reiser, G. (2006) Opposite diastereoselective activation of P2Y₁ and P2Y₁₁ nucleotide receptors by adenosine 5'-O-(alpha-boranotriphosphate) analogues. *Br. J. Pharmacol.* **149**, 416-423
 - 49 Qi, A. D., Kennedy, C., Harden, T. K. and Nicholas, R. A. (2001) Differential coupling of the human P2Y₁₁ receptor to phospholipase C and adenylyl cyclase. *Br. J. Pharmacol.* **132**, 318-326

- 50 Strudwick, N., Bhogal, N., Evans, N. A., Blaney, F. E. and Findlay, J. B. (2004) Evidence to support a spectrum of active states for the glucagon receptor. *Biochem Soc Trans* **32**, 1037-1039
- 51 Ahmed, M., Muntasir, H. A., Hossain, M., Ishiguro, M., Komiyama, T., Muramatsu, I., Kurose, H. and Nagatomo, T. (2006) Beta-blockers show inverse agonism to a novel constitutively active mutant of beta1-adrenoceptor. *J Pharmacol Sci* **102**, 167-172
- 52 Biebermann, H., Schoneberg, T., Hess, C., Germak, J., Gudermann, T. and Gruters, A. (2001) The first activating TSH receptor mutation in transmembrane domain 1 identified in a family with nonautoimmune hyperthyroidism. *J Clin Endocrinol Metab* **86**, 4429-4433

Figure Legends:

Fig. 1: Alignment of *hP2Y*-R domains that comprise the binding pocket. Code: residues that are conserved in all GPCRs – grey highlight; conserved in all *hP2Y*-R – italic letters, identical/similar in *hP2Y_{1,11}*-R – underlined. Residues proposed to be involved in ligand binding at the *hP2Y₁₁*-R – bold. (see also: supplementary material for a colour coded image).

Fig. 2: A list of known *hP2Y₁₁*-R agonists with respective EC₅₀ values for IP₃ elevation given in the Table, as reported by Communi et al. [5].

Fig. 3: Results of virtual screening of the drug-like compounds, random nucleotides and *hP2Y₁₁*-R agonists data sets on the *hP2Y₁₁*-R model. An enrichment factor of 5 was obtained, thus validating the calculated *hP2Y₁₁*-R model. Code: random ligand recovery – black line, enrichment obtained with the *hP2Y₁₁*-R model – grey line.

Fig. 4: A: *hP2Y₁₁*-R model, B: *hP2Y₁*-R model, C: b-rhodopsin. Residue color code: Blue – Arg, Lys; Red – Asp, Glu; Yellow – Pro. Loops of the *hP2Y₁₁*-R were not modelled accurately.

Fig. 5: Binding mode of ATP at the *hP2Y₁₁*-R. Major binding interactions include ionic interactions with the triphosphate chain – Arg106, Arg268 and Arg307; H-bonding interaction with P_γ – Ser206; π -stacking interaction with the adenine ring – Phe109, and interaction with Met310. (See also Table 2)

Fig. 6: The hydrophobic pocket (yellow) present in the vicinity of the C2-position of ATP in the *hP2Y₁₁*-R model (A) and in the *hP2Y₁*-R model (B). This pocket in the *hP2Y₁₁*-R is situated between TM2 and TM7, and is confined by residues Leu82 (TM2), Phe109 (TM3), Leu113 (TM3), Pro311 (TM7), and Ala313 (TM7). In the *hP2Y₁*-R model, the hydrophobic pocket is comprised of Leu104, Pro105, Ile130, Val133, and Leu135.

Fig. 7: Concentration-response curves for ATP in inducing intracellular [Ca²⁺]_i rise in 1321N1 cells stably expressing the wild type and mutant P2Y₁₁-GFP receptors. Cells

preincubated with 2 μ M fura-2-AM were stimulated with varying concentrations of ATP and the change in fluorescence ($\Delta F_{340\text{nm}}/F_{380\text{nm}}$) was detected. Data represent the mean values and standard error of the mean from 40 to 70 single cells. Results were obtained in at least three separate experiments. Filled circles (●) represent data obtained with the wild type receptor, open circles (○) the Phe109Ile mutant, filled triangles (▼) the Glu186Ala mutant, open triangles (▽) the Arg268Ala mutant, filled squares (■) the Arg268Gln mutant and open squares (□) the Ala313Asn mutant receptor.

Fig. 8:

Intracellular cAMP content determined at basal level and after stimulation with ATP (100 μ M, 1 mM) in 1321N1 cells stably transfected with the wild type *hP2Y₁₁*-R, and mutant receptors, respectively. cAMP was determined after 10 min incubation with ATP in cellular extracts by a cAMP-EIA. Bar graphs show the mean and standard error from four separate experiments.

Tables

Table 1

Identity (upper triangle) and similarity (lower triangle) percentages between various hP2Y-Rs (number n) and b-Rhodopsin for the TM domains only.

<i>hP2Y_n</i> \ <i>hP2Y_n</i>	14	13	12	11	6	4	2	1	b-Rh
b-Rh	16	21	20	21	19	20	22	23	100
1	31	29	26	38	44	49	45	100	54
2	30	29	28	36	49	67	100	76	52
4	33	29	30	37	49	100	87	77	51
6	29	28	26	33	100	75	75	71	50
11	23	22	23	100	68	68	68	72	52
12	57	57	100	52	59	56	55	54	43
13	53	100	77	50	56	53	53	54	46
14	100	73	75	57	60	62	58	62	48

Table 2

List of amino acid (aa) residues in *hP2Y₁₁*-R, and the corresponding residues in *hP2Y₁*-R, which participate in ATP recognition.

TM: transmembrane domain.

aa residue in <i>hP2Y₁₁</i> -R	homologous aa residue in <i>hP2Y₁</i> -R	TM	ATP	Distance of the <i>hP2Y₁₁</i> -R aa residue from ATP(Å)
Arg106	Arg128	3	P α,γ	3.05, 2.63
Phe109	Phe131	3	Adenine	3.61
Ser206	Ser218	5	P γ	2.60
Arg268	Lys280	6	P β	2.66
Arg307	Arg310	7	P α	2.66
Arg307	Arg310	7	N ⁶ -H	2.07
Met310	-	7	Adenine	3.54

Table 3

Intracellular calcium release induced by stimulation of mutant *hP2Y₁₁*-GFP receptors and expression levels of mutant receptors. Data represent mean EC₅₀ values (μM) ± s.e.m., obtained from n (numbers) concentration response curves of 1321N1 cells stably expressing the wild type or mutated receptor. The receptor expression level was derived from n experiments.

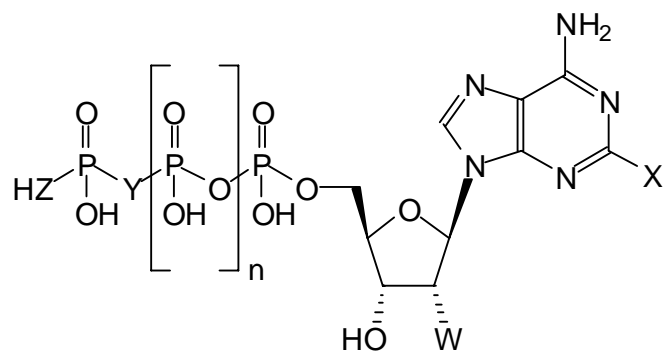
<i>hP2Y₁₁</i> -R construct	residue	EC ₅₀ value (μM)		Receptor expression level (%) (n)
		ATP	ATPγS	
wt		2.37±0.88 (4)	1.04±0.38 (4)	100
R106A	3.29	^a	n.d.	76.1±4.7 (4)
F109I	3.32	10.7±2.29 (5)	n.d.	102±13 (7)
E186A	EL2	32.8±21.1 (5)	4.92±1.07 (4)	111±10 (9)
Y261A	6.48	^a	n.d.	77.4±3.9 (4)
R268A	6.55	1806±354 (3)	247±178 (8)	143±23 (3)
R268Q	6.55	102±20 (5)	10.3±2.59 (3)	95.6±8.0 (7)
R307A	7.39	^a	n.d.	87.5±5.9 (4)
A313N	7.45	4.52±0.99 (7)	n.d.	97.6±11.9 (4)

^a ATP induced no significant increase in intracellular calcium up to concentrations of 10 mM. n.d. – not determined.

Figures

TM3		
	99	131
P2Y ₁₁	<u>EAACRLERFLFTCNLLGSVIFITCISLNRYLGI</u>	
P2Y ₁	<u>DAMCKLQRFIFHVNLVYGSILFLTCISAHRYSGV</u>	
P2Y ₂	<u>TVLCKLVRFLEYTNLYCSILFLTCISVHRCLGV</u>	
P2Y ₄	<u>TEICKFVRFLFYWNLYCSVLFLTCISVHRYLGI</u>	
P2Y ₆	<u>DFACRLVRFLFYANLHGSILFLTCISFQRYLGI</u>	
Rhodopsin	<u>PTGCNLEGFFATLGGEIALWSLVVLAIERVVV</u>	
	107	139
EL-2		
	167	201
P2Y ₁₁	<u>FSHLKRPQQGAGNCSVARPEACIKCLGTADHGLAA</u>	
P2Y ₁	<u>YSGTG-VRKNKTITCYDTTSDEYLRS</u>	
P2Y ₂	<u>FVTTS-ARGG-RVTCHDTSAPELFSR</u>	
P2Y ₄	<u>FVTTS-NKGT-TVLCHDTTRPEEFDH</u>	
P2Y ₆	<u>FAATG-IQRN-RTVCYDLSPPALATH</u>	
Rhodopsin	<u>GWSRYIPEGMQCSCGIDYYTPHEETN</u>	
	174	199
TM6		
	243	269
P2Y ₁₁	<u>KLRVAALVASGVALYASSYVFPYHIMRV</u>	
P2Y ₁	<u>RRKSIYLVIIVLTVFAVSYIPFHVMKT</u>	
P2Y ₂	<u>R-KSVRTIAVVLAVFALCFLPFHVTRT</u>	
P2Y ₄	<u>L-RSLRTIAVVLTVFAVCFVPFHITRT</u>	
P2Y ₆	<u>RGKAARMAVVVAAAFAISFLPFHITKT</u>	
Rhodopsin	<u>EKEVTRMVIIMVIAFLICWLPYAGVAF</u>	
	247	273
TM7		
	301	321
P2Y ₁₁	<u>VGYQVMRGLMPLAFCVHPLLY</u>	
P2Y ₁	<u>ATYQVTRGLASLNSCVDPILY</u>	
P2Y ₂	<u>MAYKVTRPLASANSCLDPVLY</u>	
P2Y ₄	<u>VVYKVTRPLASANSCLDPVLY</u>	
P2Y ₆	<u>AAYKGTRPFASANSVLDPILF</u>	
Rhodopsin	<u>IEMTIPAEFAKTSAVYNPEVIY</u>	
	286	306

Figure 1



#	n	W	X	Y	Z	Name	EC ₅₀ (μM) IP ₃ elevation ^a
1	1	OH	PrS	CCl ₂	O	AR-C67085	8.9
2	1	Bz	H	O	O	Bz-ATP	10.5
3	1	OH	H	O	S	ATP-γ-S	13.5
4	1	H	H	O	O	2'-dATP	16.3
5	1	OH	H	O	O	ATP	65
6	0	OH	H	O	S	ADP-β-S	174
7	1	OH	MeS	O	O	2-MeS-ATP	210

^a ref 5.

Figure 2

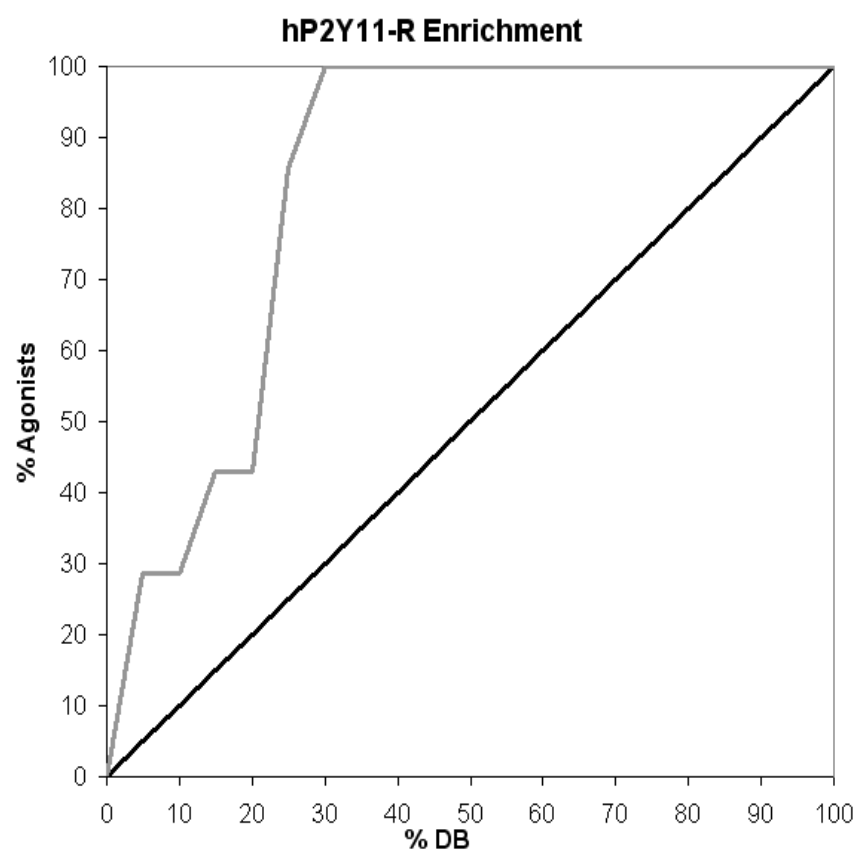


Figure 3

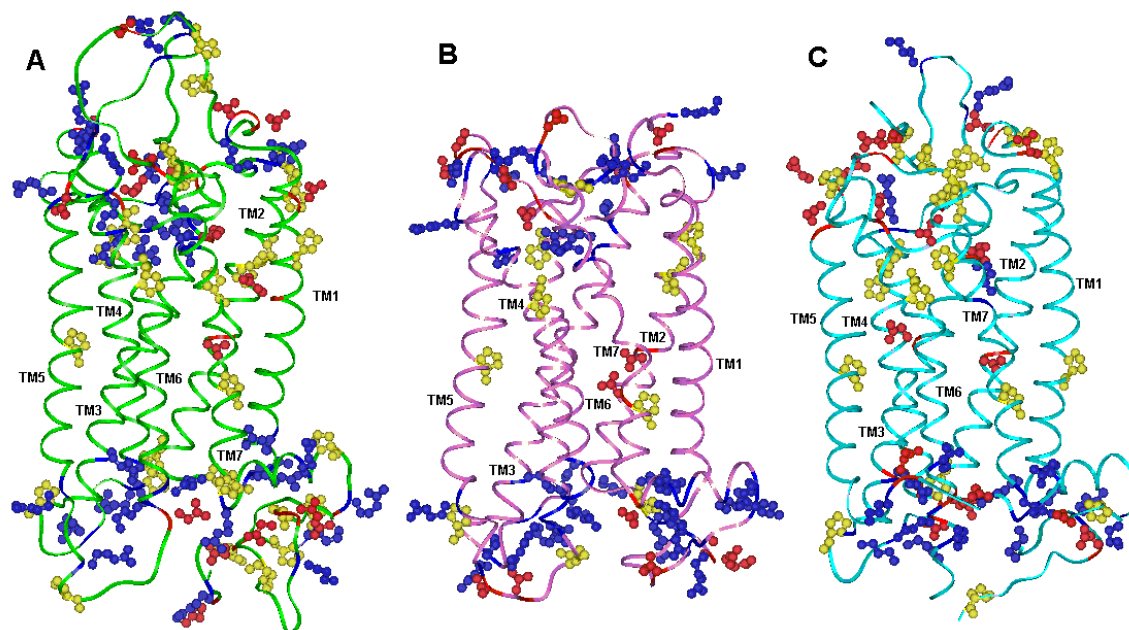


Figure 4

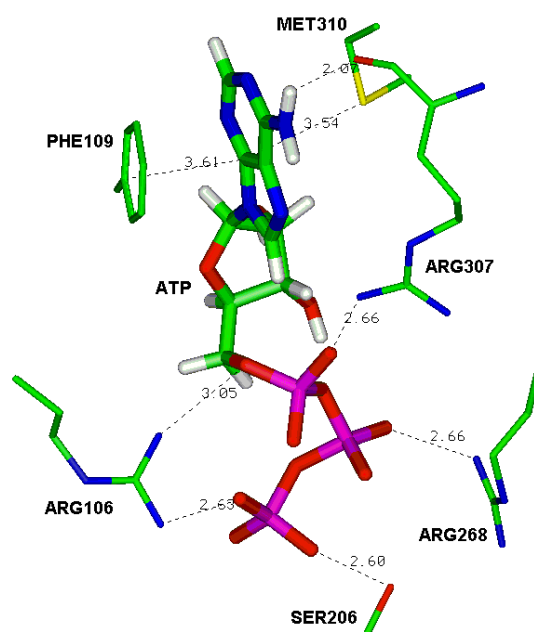


Figure 5

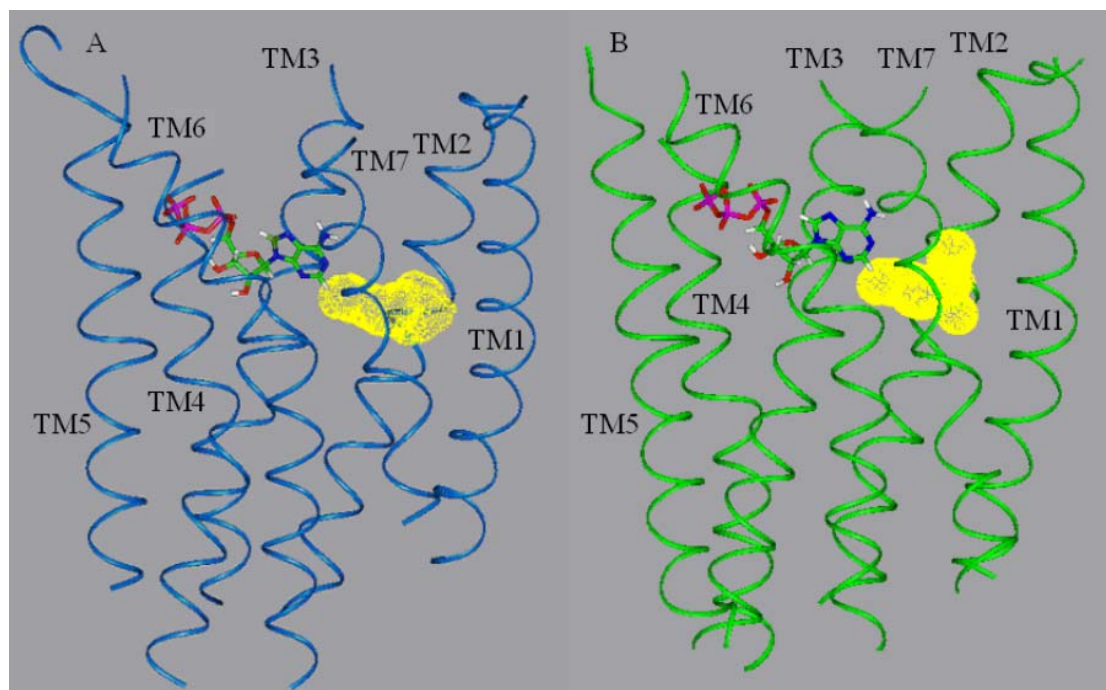


Figure 6

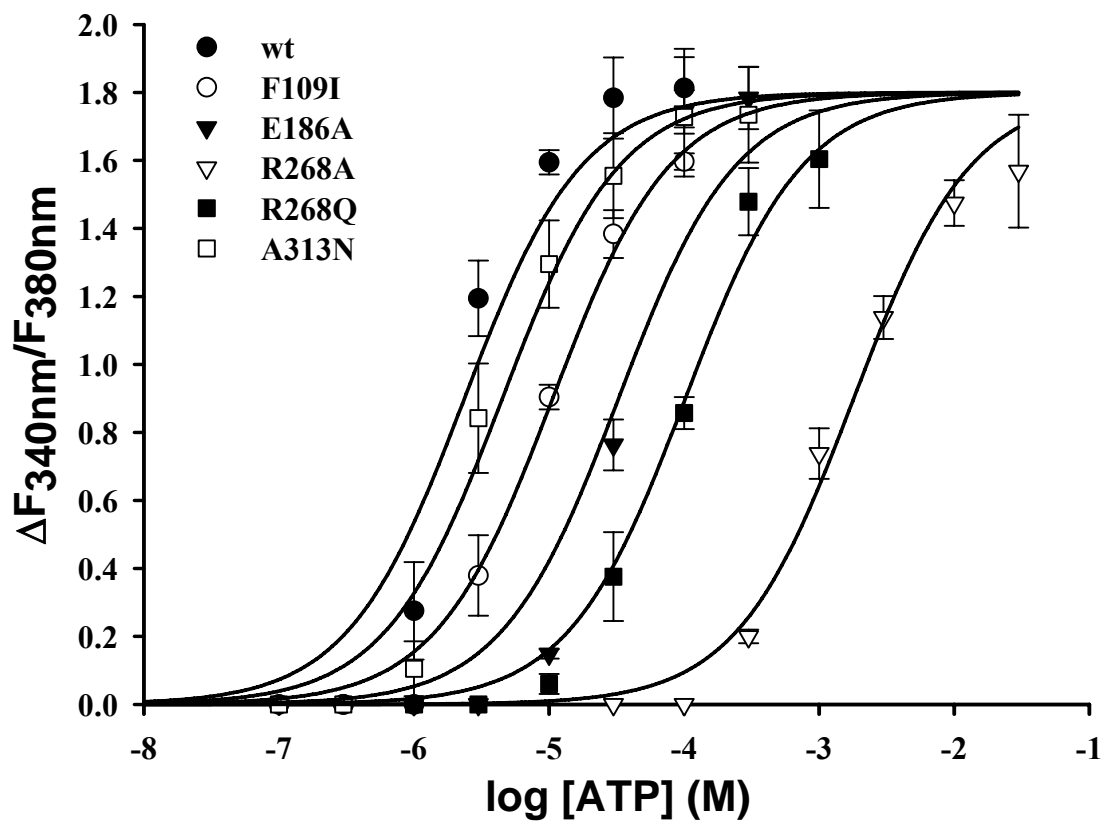


Figure 7

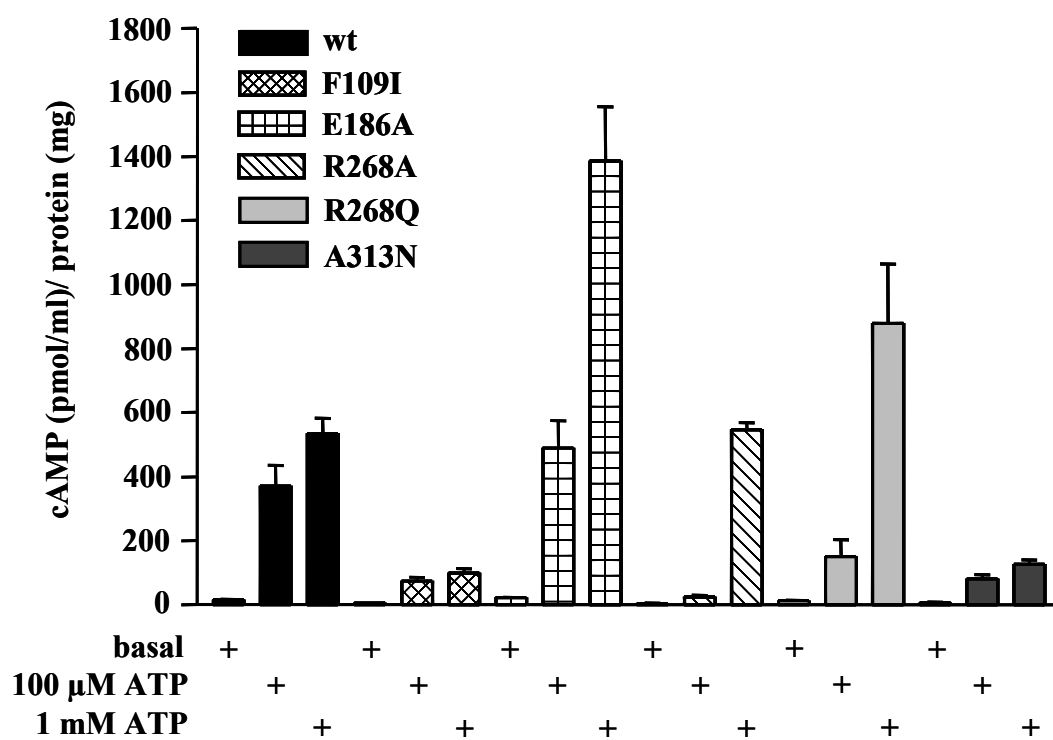


Figure 8